arXiv:1402.6857v1 [cond-mat.supr-con] 27 Feb 2014

Advanced superconducting circuits and devices

To be published in *Handbook of Applied Superconductivity*, Wiley-VCH

Martin Weides and Hannes Rotzinger
Physikalisches Institut, Karlsruher Institut für Technologie, Germany

Contents

1 Field effect devices **2**
1.1 Josephson field effect transistor 2
1.2 NanoSQUIDs 2
1.3 Majorana fermions and topological qubits 3

2 Quantum information circuits **5**
2.1 Material and design considerations 6

3 Metamaterials at microwave frequencies **6**
3.1 Classic metamaterials 7
3.2 Quantum metamaterials 8

4 Quantum Phase Slips **8**
4.1 Basic concept 8
4.2 Phase slip flux qubit 10
4.3 Constant current steps 11

The unique properties of superconducting devices like ultra low power consumption, long coherence, good scalability, smooth integration with state of the art electronics and in combination with the Josephson effect outstanding magnetic field sensitivity, suits them well for a wide range of applications. Questions in fundamental and applied disciplines, like material characterization, particle detectors, ultra-low loss microwave components, medical imaging, and potentially scalable quantum computers are commonly addressed.

Using integrated-circuit processing techniques, adapted from the semiconductor industry, complex micron or nanometer sized electronic circuits elements can be scaled up to large numbers. Examples for such devices are for instance, SQUID or microwave resonators. SQUIDs (superconducting quantum interference devices) are high resolution magnetometers, sensitive enough to measure the extremely small magnetic fields originating, for example, from the human brain activity or single molecules.

Recent advances in thin film technology have made it possible to fabricate compact superconducting microwave resonators with a tremendous frequency purity. The developments towards such devices have been triggered by the requirement of storing the quantum information of a quantum bit as long as possible in an unperturbed way, since superconducting quantum circuits are one of the most promising systems to fulfill the DiVincenzo criteria [1] for a scalable quantum computer.

Not only the quantum computing science is benefitting from this progress, but also other fields with functional micro and nano-structures in the ultra-low noise environment of low temperatures. For instance, coupled cavity-qubit experiments showed the validity of cavity quantum electrodynamics for microwave photons with these circuits such as dressed states or coherence. Parametric amplification of microwave signals was shown using a tunable resonator with an added noise temperature well below 1 Kelvin. Also very promising is the frequency domain multiplexing of many highly sensitive particle detectors each coupled to a superconducting resonator with a slightly different frequency. This approach allows for an energy sensitive particle camera with many pixels, being read-out by a single microwave line.

In the following we give an overview on superconducting circuits with new functionalities in the classical and quantum regime. We will start with a brief overview of novel devices based on nanoscale semiconducting Josephson barriers. Second, the fast-developing field of quantum computing is discussed with a focus

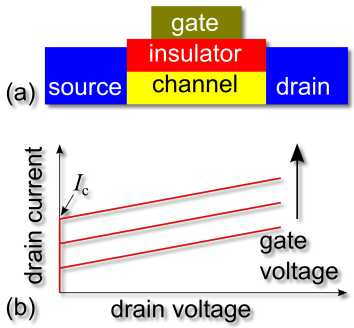

Figure 1: **a)** Schematics of a Josephson field effect transistor. The critical current I_c, and for larger source-drain currents the voltage between source and drain are modulated inside the channel by a voltage on the gate electrode. The insulator suppresses the leakage currents from the gate metal. **b)** Current-voltage characteristic of the source-drain channel as function of voltage bias on the gate electrode.

on limitations, challenges, and opportunities. This is followed by a section on superconducting metamaterials and its applications at microwave frequencies in the classical and quantum regime. We conclude with an introduction in quantum phase slip junctions and its potential being useful complementary to the Josephson junction.

1 Field effect devices

1.1 Josephson field effect transistor

Field-effect superconducting devices use an applied electric field, and not the magnetic flux as normally done for conventional Josephson circuits, to control the coupling between the superconducting electrodes. Basic parameters, such as the critical current I_c, plasma frequency or characteristic voltage, see Fig. 1 can be in-situ modified. The field-effect changes the Josephson coupling across a semiconducting material, for instance with an applied voltage. The effect is fundamentally different from the electrostatic tuning of the transport properties of small capacitance Josephson devices in the Coulomb blockade / charge regime, which are for instance used for superconducting single electron tunneling devices or the charge qubit.

Josephson field-effect-transistors operate in the phase regime and are controlled by a gate electrode being galvanically decoupled from the junction by either a dielectric or a Schottky barrier [2]. I_c and, for larger source-drain currents, the source-drain voltage are modulated as function of the gate voltage. Tunability was demonstrated for devices based on inversion layers, two-dimensional electron gases, nanowires and nanotubes. The superconductor/semiconductor interface transparency is critical, especially for silicon based semiconductors. They tend to form a Schottky barrier, unless very high doping concentrations (with reduced field-effect) are used. For voltage gain the output voltage across the source-drain channel must exceed the control voltage applied at the gate. Josephson field-effect transistors have been fabricated based on semiconducting interlayer [3], channel [4], or wire [5–9] barriers. These systems have considerable potential for low-loss, fast digital elements as well as for analog applications such as cryogenic voltage amplifiers.

1.2 NanoSQUIDs

Conventional SQUIDs (compare chapter 9) are made from Josephson tunnel junctions embedded in a closed loop with the junction's lateral dimensions being on the order of microns. Replacing the tunnel junctions with nano-scale Josephson junctions the noise performance can be enhanced [10] and single atomic spin measurement can be achieved [11]. The detection of a single molecule's magnetic moment requires a substantial fraction of the particle's magnetic field to penetrate the SQUID loop. Choosing a

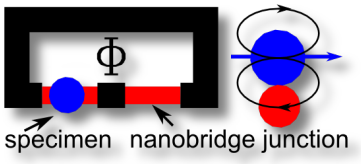

Figure 2: **Left:** A nanoSQUID with nanobridge Josephson junctions (red) having similar dimensions as the magnetic specimen (blue) under investigation. **Right:** Strong coupling of magnetic flux (black lines) from the specimen to the Josephson junction and SQUID loop (black) underneath significantly affects the sensed flux Φ through the DC SQUID loop. The nanoSQUID signal is detected either by transport or by microwave reflectometry.

nanoSQUID [12], as depicted in Fig. 2, the magnetic specimen can be placed above one of the Josephson junctions of similar dimensions. Thereby the coupling of magnetic flux to the loop is optimized.

The nanobridge junctions are typically formed by a superconducting constriction with a normal or semiconducting barrier made by thin films, nanowires or nanotubes. The nano-size dimensions are realized by patterning methods such as focused ion beam etching, electron beam or atomic force microscopy lithography on lateral films. The interest in nanoSQUIDs goes well beyond the magnetic field detection. When using semiconductor barriers, e.g. carbon nanotubes [13] or nanowires such as indium arsenide [6], the junction behaves as a quantum dot with well-separated electronic levels due to the exciton confinement in all three spatial dimensions. The position of the quantum levels can be tuned with an applied gate voltage similar to the Josephson field-effect barriers described in the previous section. Thereby a gate-controlled transition from the normal (0-type) to the π-Josephson junction can be observed (see chapter 1) depending on the electron parity in the constriction. These junctions have a Josephson phase $\phi = \pi$ in the ground state when no external current or magnetic field is applied, and a negative critical current I_c with the first Josephson relation being modified to $I_s = -|I_c| \sin(\phi) = |I_c| \sin(\phi + \pi)$.

1.3 Majorana fermions and topological qubits

Another field of significant interest are semiconducting nanowires controlled by local gates and proximitized by a superconductor. They receive considerable attention in the quest for Majorana fermions and topological qubits. Majorana fermions are fermionic quasiparticle excitations which are their own anti-particles [14].

Majorana fermions are expected to be located in conductive nanowires contacted with superconductors. In the proximitized region they may emerge as non-fundamental quasiparticles at zero-energy. Since the Fermi level is in the middle of the superconducting gap, these midgap states can be realized by conventional thin films technology, nanowires of semiconductors [15, 16] or metals [17] with a pronounced spin-orbit coupling. An external magnetic field B is applied to make the band appear spinless. For certain electron densities, the combination of the induced superconducting gap, the strong spin-orbit coupling in the nanowire and the magnetic field open an unconventional superconducting state with Majorana bound states at its ends, see Fig. 3. Recently, its signature was reported based on electrical measurements on an indium antimonide nanowire-superconductor hybrid structure [18] where gate electrodes modified the electronic structure of the nanowire exposed to a magnetic field. In transport measurements across the tunnel barrier from the normal metal to the superconductor, the conductance close to zero voltage is enhanced by the presence of Majorana states next to the tunnel barrier.

A different class of qubits are potentially decoherence-free topological qubits. Conventional superconducting qubits such as superconducting flux, phase or transmon qubits have been implemented and coherence times about 100μsec achieved by optimal control of their electromagnetic environment and intrinsic sources of decoherence. The alternative qubit approach is, for example, based on the fermionic state formed by a combination of two Majorana particles. Due to the intrinsic topological protection from decoherence, the need for error correction is expected to be minimal [19].

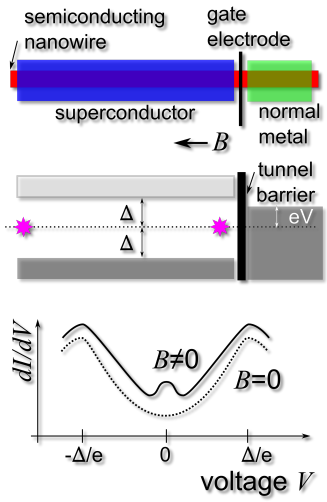

Figure 3: **Top:** The nanowire with strong spin-orbit coupling is proximity coupled to a bulk superconductor and a normal metal. A gate voltage establishes a tunneling barrier at the interface between the metallic and superconducting parts of the wire. An applied magnetic field B parallel to the wire induces two Majorana fermions (depicted as stars) as quasiparticles on both interfaces. **Middle:** For bias voltages V smaller than Δ/e electrons from the normal metal cannot tunnel into the wire. In case a Majorana state is located near that tunnel barrier, electron tunneling into the wire's Fermi level is allowed. **Bottom:** The differential conductance dI/dV across normal-metal and superconducting electrodes as a function of applied bias voltage V shows a local maximum at zero voltage indicating the emergence of a Majorana fermion inside the gap and next to the tunnel barrier.

2 Quantum information circuits

Superconducting quantum information circuits are promising solid state candidates as building elements for quantum computers due to ultra-low dissipation, inherent to superconductors. The key element, the superconducting qubit, exists in three basic types as charge [20], flux [21] and phase qubit [22]. All of these first generation qubits may fulfill the five DiVincenzo criteria [1] for a scalable quantum computer but are limited by low coherence.

Depending on the Josephson over charging energy ratio E_J/E_c (with $E_J = \Phi_0 I_c/2\pi$ and $E_c = e^2/2C$) their coherence is affected by either charge noise (ultra-small capacitors, $E_c \gg E_J$), or dielectric loss (large capacitors, $E_c \ll E_J$). The second generation of superconducting qubit concepts (developed in the time from 2002 till 2010) are based on hybrid qubits to minimize these environmental influences. For instance, the charge-flux [23], low impedance flux qubits [24], less flux-noise sensitive [25] and even a charge-insensitive Cooper pair box [26] qubit have been realized.

For the third qubit generation, currently under development, the residual loss is being pushed below the threshold for quantum error correction. Advancement strategies involve scaling the qubit dimensions up to reduce the inevitable surface loss participation and employing better material with less dielectric surface states.

In fifteen years, impressive progress has been made to address, control, readout, and scale superconducting qubits, resulting, for example, in the proof of the violation of Bell's inequality, measurements of three qubit entanglement, quantum non-demolition readout, creation of arbitrary photon states, and circuit quantum electrodynamics in strong and ultra-strong coupling regimes.

In general qubits are limited by intrinsic decoherence processes which return an excited state to the ground state. In the Bloch picture of a two-level state, the energy relaxation time T_1 describes the longitudinal and the dephasing time T_2 the transverse relaxation. The physical origin for decoherence is attributed to, among others, coupling to discrete or continuum electronic defect states, flux or charge noise, or pair-breaking radiation.

The building blocks of quantum circuits are quantum gates operating on a small number of qubits. The quantum gate error budget has contributions from decoherence processes occurring during the gate operation such as signal noise or off-resonant excitations. Quantum error correction theory predicts that once the error rate of individual quantum gates is below a certain threshold, all errors can be corrected by concatenated quantum codes. These are based on stabilizer codes employing additional qubits (called

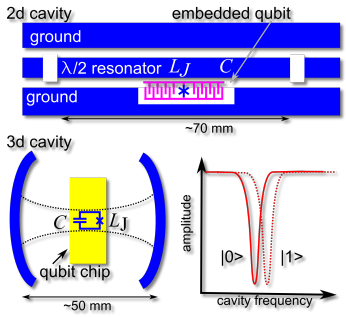

Figure 4: Schematic of a qubit (here a transmon qubit) inside a 2d (**top**) or 3d (**bottom left**) cavity. Dielectric loss is reduced by better materials (2d implementation) or less surface dielectric contribution (3d implementation). The quantized cavity states suppressed the qubit coupling to the electromagnetic continuum giving rise to spontaneous emission. **Bottom right:** The cavity response depends on the state of the dispersively coupled qubit ($|0\rangle$, $|1\rangle$) and is used for the qubit readout. While the 2d and 3d cavities have similar dimensions the 2d cavity can be meandered to reduce its footprint significantly. The resonator/qubit dimensions are not to scale.

ancilla qubits) coupled to the qubit of interest and thereby forming highly entangled, encoded states to correct for local noisy errors. By encoding one logical qubit in several physical qubits one can correct for bit flip or/and sign flip errors in the single logical qubit. As of 2013, the error correction threshold is achieved by the first superconducting quantum bits.

2.1 Material and design considerations

Superconducting qubits consist of linear (capacitor, inductor) and non-linear (Josephson junction inductance) circuit elements. One limiting coherence factor is the employed thin film materials. In a resonant circuit the energy stored is $E_{\rm total}$, where on average the capacitive energy equals the inductive energy. The lifetime $T_1 = 1/\delta_{\rm m} 2\pi f_q$ at the qubit frequency f_q is a measure of the relative energy loss $\delta_{\rm m} = \Delta E/E_{\rm total}$ per cycle time defined as

$$\delta_{\rm m} = \frac{\Delta E}{2\pi E_{\rm total}} = \frac{\Delta E_C + \Delta E_L}{2\pi E_{\rm total}} = \delta_C + \delta_L \ . \tag{1}$$

Loss can be separated into contributions from the capacitive (δ_C) and inductive (δ_L) circuit elements. Superconducting qubits have been optimized by identifying the local contributions of capacitive and inductive losses to the linear and non-linear elements. The linear elements have been directly improved by considerable research activities on microwave kinetic inductance detectors [27]. Progress in material research [28–30] and resonator surface [31] led to Al, Re, TiN being the lowest-loss thin film superconducting resonators. Sapphire and undoped (high resistivity) silicon wafers are used as low-loss substrates.

The non-linear Josephson inductance, providing the qubit's anharmonicity, is conventionally formed by oxygen diffused, amorphous and defect-rich $\mathrm{Al}\emptyset_x$ tunnel junctions. A major contributor to relaxation processes in superconducting qubits originates from dielectric (i.e. capacitive) loss caused by microscopic two-level systems (TLS) in amorphous layers such as the surface oxide or tunnel barrier. TLS are commonly attributed to atoms or groups of atoms tunneling between two configuration states. The resonant response of an ensemble of TLS in a microwave field is found to decrease the coherence due to microwave absorption. A small volume of the tunnel barrier or surface oxide layers implies that most operation frequencies do not put the qubit on resonance with these two-level systems. The tunnel junction loss contribution can be statistically avoided by scaling the non-linear $\mathrm{Al}\emptyset_x$ tunnel junction down to tenths of microns dimensions. The surface loss arising from coupling to native oxides of a few nanometer thickness at the vacuum or substrate interfaces is suppressed by scaling the circuity up to a millimeter size and thereby reducing the electric field across, and the coupling to defect states within these oxides.

For example, the 3d transmon [32] uses a shunting capacitance C with negligible surface loss due to the large electrode separation and ultra-small tunnel junction areas, see Fig. 4. By placing the qubit chip in a machined microwave cavity of millimeter dimension the quantized mode spectrum protects the qubit from radiative electromagnetic loss and the bulk metal enclosure screens the pair-breaking blackbody radiation from higher temperature surfaces. 3d qubits were shown to have T_1 times above 100 μsec. While their large volume per qubit may limit scalability beyond a certain number of qubits today's few-qubit experiments on quantum gates or quantum algorithms can be implemented directly and tested. Good scalability is expected from 2d qubit implementations as the resonator with the embedded qubit can be wrapped on the chip surface to reduce the footprint significantly. An increase in coherence is achieved by improved materials for capacitors, inductors and Josephson junctions. For example capacitors with electrodes having less interface oxides were shown to raise the qubit lifetime to the same order achieved by the 3d qubit. The absence of a quantized mode spectrum in the third dimension requires a well elaborated geometry design to tailor the electromagnetic environment.

3 Metamaterials at microwave frequencies

Metamaterials are artificially engineered structures with electromagnetic properties that are not found in nature. The most striking example of such properties is a negative index of refraction, analyzed first in a theoretical work in 1967 [33] and experimentally realized in 2001 in arrays of split-ring resonators [34, 35]. Negative real parts of both dielectric permittivity ϵ and magnetic permeability μ can be realized by

working at frequencies near a resonance of an artificial electromagnetic material resonator. For example in metals close to the plasma resonance, the permittivity is positive below and negative above the resonance. Below the resonance frequency, the waves oscillate slowly enough for the electrons to follow, and above the resonant frequency, the inertia of the electrons prevents the electrons from oscillating in proper phase with the incident wave. In such a negative index material, the energy propagation (expressed by the Poynting vector $\vec{S}$) is opposite to the direction of the phase for a traveling plane wave. Such materials are often referred to as being 'left handed' as the electric and magnetic fields, and the direction of propagation of the electromagnetic wave obey the left-hand rule. A lossless negative-index material would, in principle, allow an imaging resolution well below the diffraction limited by focusing the entire spectrum containing both the propagating as well as the evanescent spectra.

However, in conventional, metallic, nanostructures the resonant current enhancement causes significant losses limiting the electric field amplification. The resonance frequency is determined by the geometry, thus complicating the frequency tunability. Using superconducting resonators with Josephson junctions as tunable, non-linear inductors allows improving the performance by adding high amplification and a broad tunable microwave range.

3.1 Classic metamaterials

The superconducting version of the conventional split-ring resonator based metamaterial is a two-dimensional array of SQUID arrays. Such an array exhibits large negative magnetic response above the resonance frequency and the frequency is tuned by an external perpendicular magnetic field. In first experiments superconducting niobium split-ring resonators showed evidence of negative effective permittivity, permeability, and a negative effective index pass-band in the superconducting state at GHz frequencies [36]. A nonlinear left-handed transmission line can be formed by Josephson junctions as shunt inductances. One-dimensional Josephson junction arrays (see sketch in Fig 5) with generalized unit cells allow to engineer the band gaps in the electromagnetic spectrum in full analogy to electronic band gaps in crystals. Frequency-tunable right- and left-handed linear and nonlinear dispersion relation element can be merged for novel and innovative conceptual advance of microwave elements and devices. A tunable metamaterial was realized in a SQUID chain that operates in the lower GHz frequency band [37]. This general-purpose parametric device is capable of squeezing the quantum noise of the electromagnetic vacuum. Squeezed states, having less uncertainty in one observable than the vacuum state are used for enhanced precision measurements. For instance amplitude-squeezed light improves the readout of very weak spectroscopic signals, while phase-squeezed light improves the phase readout of an interferometer. The parametric oscillator is used for low-noise amplifiers, for example for quantum-state qubit readout in the microwave domain and quantum non-demolition measurements.

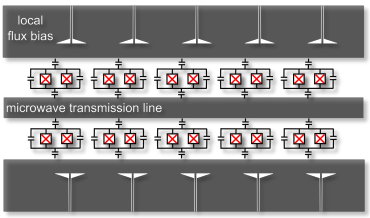

Figure 5: Sketch of a chain of DC SQUIDs or qubits placed at evenly spaced intervals and uniformly coupled to the center conductor of a coplanar waveguide. Each element has an individual flux bias for selective control of its transition frequency. The wave propagation in the transmission line may be reversed, and contrary to the direction of energy flow. Frequency tuning of the band gaps is achieved inductively via a DC current in the center conductor of the waveguide or magnetic coils (on-chip or external).

3.2 Quantum metamaterials

Besides the above-mentioned promising improvements of known metamaterial functionalities through reduced losses and frequency tunability, superconducting metamaterials offer a major novel and potentially disruptive properties that originates from their quantum properties. The quantum electromagnetic properties of such superconducting qubits can be controlled and tuned by external DC magnetic fields. The experimental realization of controlled coupling between the quantum electromagnetic field and chain/arrays of qubits that evolve quantum-coherently with the field may open practical routes towards the very exciting field of quantum metamaterials. For instance, superconducting quantum metamaterials could be realized through tailored chains of qubits that are embedded into superconducting transmission-line resonators. This opens entirely novel opportunities such as the realization of lasing with very few (or even just one [38]) qubits.
First thoughts of using macroscopic superconducting quantum metamaterial have been suggested in theoretical works. For the quantum version of SQUID arrays as a left-handed metamaterial the quantum expressions for the associated negative refractive index was derived in Ref. [39]. The propagation of a classical electromagnetic wave through a transmission line formed by superconducting qubits embedded in a superconducting resonator was considered in Ref. [40]. In particular, the spectroscopic properties of such a quantum Josephson transmission line will be controlled by the quantum coherent state of the qubits. And a chain of qubits coupled the transmission line can modify the band-gap structure to slow and stop the microwave propagation [41].

A single qubit coupled to a harmonic oscillator is described by the Jaynes-Cummings [42, 43] model, and it's generalization to many qubits not interacting with each other is given by the Tavis-Cummings model [44]. This model provides the framework to study collective properties of the qubits for the coherent transmission of microwave photons through a microwave resonator coupled to tunable qubits periodically placed in the gap and capacitively coupled to the resonator. The Dicke model [45] describes the coupling between such a collection of two-level systems and a single photon mode. For increasing light-matter coupling the model predicts excitons giving rise to many cooperative radiation phenomena such as superradiance and super-fluorescence [46]. The counterpart of the collective excited state radiative decay is a destructive interference effect, termed subradiance, leading to the partial trapping of light in the system. Adding qubit nearest-neighbor interaction in linear chains of Josephson qubits leads to interesting dynamical entanglement properties of coupled many-body systems [47]. Multiple superconducting qubits can coupled identically to the field mode of the same cavity, for example by optimizing the placement of qubits at field antinodes of a distributed resonator [48]. For large couplings both superradiant microwave pulses and phase multistability are expected. In the case of non-uniform coupling rates subradiant transitions are induced [49]. The resulting excitation spectrum depends on the amount the inhomogeneous system deviates from the homogeneous case, and crosses from Frenkel- to Wannier-type (i.e. localized to non-localized) excitons for increasing larger distances in the superconducting qubit chain.
From an experimental point of view, the coherent quantum dynamics of superconducting qubits coupled to the electromagnetic field in a transmission line opens novel opportunities for material-induced coherent transformation (e.g. light squeezing, coherent down- and up-conversion, etc.) of incident radiation. Resonance fluorescence [50] and electromagnetically induced transparency [51] on an individual qubit were both observed on one qubit coupled to a transmission line. Coherent population trapping was found in a phase qubit [52]. And an electromagnetically induced transparency qubit was use to realize a single-photon router, where an incoming signal can be routed to the output port [53].

4 Quantum Phase Slips

4.1 Basic concept

In a quantum phase slip circuit, a one dimensional superconducting nano-wire is used as a non-linear element connecting two conventional superconductors. The research on phase slips has its origins in the late 1960s, where transport measurements observed a finite resistance of superconducting wires in the close

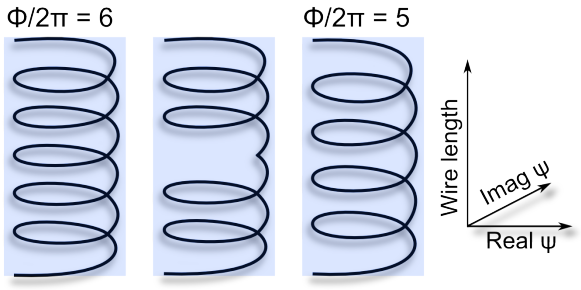

Figure 6: Ilustration of a phase slip process. In a narrow superconducting wire the accumulated phase ϕ of the order parameter can slip by 2π if the width is comparable to the coherence length.

vicinity to the superconducting transition temperature. In such a wire, phase slips of the superconducting order parameter ψ can occur if the width of the wire is comparable to the superconducting coherence length ξ. This is easy to fulfill even for moderate wire width ($\sim \mu$m) close to the superconducting transition temperature, where ξ diverges.
An applied voltage V is increasing the phase difference ϕ between the ends of the wire terminals according to $\mathrm{d}\phi/\mathrm{d}t = 2e/\hbar V$. Here, e is the elementary charge and $\hbar$ the reduced Planck constant. Without a phase slip, the number of phase turns increases until the current flow $I \sim \nabla\phi(\vec{r})$ reaches a critical value and superconductivity is lost.
In a phase slip capable superconducting wire, ψ can vanish for a short period of time over the length scale of ξ and allows to reduce the acquired phase by a 2π 'slip'. Since the phase around an elementary superconducting flux vortex is also 2π, a phase slip is equivalent to a flux vortex passing across a two or three dimensional wire.
In an energy potential picture, the two states of the wire, before and after the phase slip, have the same energy level. However, a phase slip event has to overcome the the condensation energy barrier of the superconductor. If the available energy is large enough for a thermally activated phase slip, the phase is allowed to change by passing over the condensation barrier potential. These phase slips happen as a stochastical process and are therefore dissipative. The energy transferred per phase slip is $I\Phi_0$, where $\Phi_0 = h/2e$ is the superconducting flux quantum and I the current passing through the wire.
In 1988, Giordano [54] observed a non-vanishing electrical resistance with very small (∼500 nm) In wires well below temperatures that would allow for a thermal activation of phase slips. Although the experimental conditions led to some controversies, a quantum mechanical tunneling processes was discussed to explain the data. The main idea pointed out in the publication was that the phase may not change in the low temperature regime by passing over the condensation energy barrier, but instead by quantum mechanical tunneling through it. This is in analogy to the well known macroscopic quantum tunneling process (MQT).
In the following years more experiments on superconducting nano-wires have been carried out. Noticeably the Tinkham group (e.g. [55, 56]) studied many samples. They used ultra narrow bridges of free hanging carbon nanotubes as a template for superconducting MoGe wires. Although these wires had diameters down to a few nanometer, the results could not unambiguously prove the existence of a quantum mechanical effect, still strong evidence for *quantum phase slip*, QPS, was provided. In depth analysis of the experiments and extensive theoretical efforts led to models describing the QPS process on a microscopic as well as on a macroscopic level (for a recent review, also on thermally activated phase slips, see e.g. [57]).
Briefly summarized the following is known about nano-wires exhibiting the QPS effect. The QPS coupling energy E_s depends linearly on the length of the wire in units of ξ and exponentially on the normal state resistance R_n of a wire with length ξ. Advantageous to get to the QPS regimes is therefore a material with a long superconducting coherence length ξ and a high normal state sheet resistance. Given this, wires

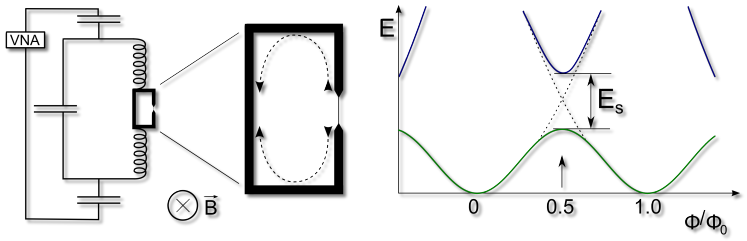

Figure 7: **Left:** Phase slip flux qubit embedded in a superconducting microwave resonator. **Right:** Energy spectrum versus applied flux. The energy of the loop without a QPS capable wire is given by the dashed black line. Quantum phase slip coupling of two neighboring flux states lifts the degeneracy at $0.5\Phi_0$ by E_s.

with a smaller diameter will allow for a higher E_s and therefore higher phase-slip rate.
QPS wires have been fabricate down to a few nanometer employing different techniques and a wide range of superconducting materials. One experimental example is given below in section 4.2

A theoretical paper by Mooij and Nazarov [58] drew a lot of attention in 2006. The authors expanded the field by deriving a fundamental duality between the Josephson and the quantum phase slip effect. Two extreme cases for both junction types are discussed:

- The Josephson junction in the superconducting state, namely the Josephson coupling energy E_J is much larger than the charging energy $E_\mathrm{c} = e^2/2C$ of the junction, C is the junction's capacitance. The junction exhibits for a supercurrent up to a critical *current* I_c without a voltage drop. This is the coherent, dissipation free regime where Josephson junctions down to a size of $\sim 1\mu\mathrm{m}^2$ are classically operated.

- Correspondingly, with the QPS energy E_s large compared to the inductive energy $E_\mathrm{L} = \phi_0^2/2L$ the QPS junction is in a strong quantum phase slip regime with no current flow up to a critical *voltage* V_c. L is the total inductance of the wire. The phase coherence along the wire is very low and therefore charge transport is suppressed.

- In the opposite Josephson junction case, $E_\mathrm{c} > E_\mathrm{J}$ and embedded in a proper environment, the system is insulating and a current flow is only admitted with the charging energy E_c provided above a critical *voltage* V_c. This is the well known regime of ultra-small Josephson junctions and arrays of ultra-small Josephson junctions with a coulomb blockade of current.

- If the QPS junctions inductive energy E_L is larger than E_s, there exists a superconducting phase coherence along the wire and a supercurrent is observable. Since the quantum phase slip energy E_s is non-zero, quantum phase slips happen at a lower rate compared to the strong phase slip regime.

It is interesting to note that the duality of JJ and QPSJ is exact with respect to the exchange of the canonically conjugated quantum variables, phase and charge. Also the existence of a kinetic capacitance in duality to the kinetic inductance of the nano-wires was predicted for QPS wires.
As a consequence of the duality of Josephson junctions and QPS junctions and previous theoretical studies [59–61] the question was raised, if it is possible to observe a dissipation free *coherent* quantum phase slip process. This is addressed in the next section.

4.2 Phase slip flux qubit

Built upon a previous work by Mooij and Harmans [62], an international collaboration around O.V. Astafiev and coworkers presented in a recent publication [63] the exact duality outlined above by exploring

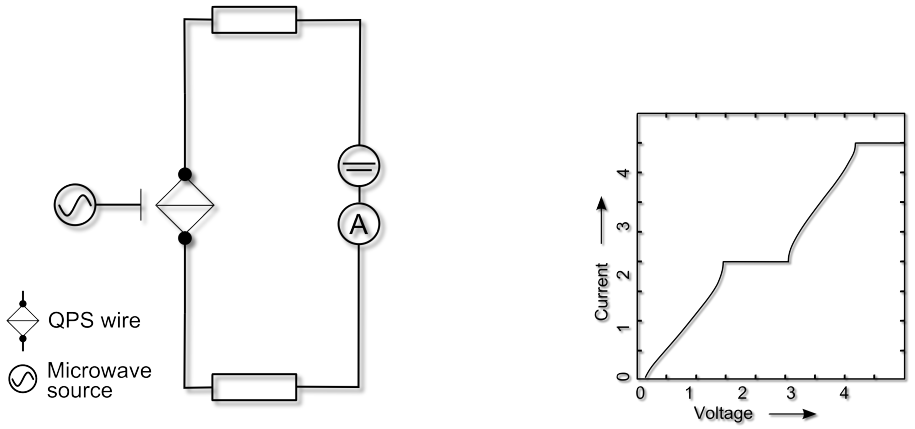

Figure 8: **Left:** Simplified schematics of a current circuit based on a QPS wire. **Right:** IV characteristics of a QPS wire under microwave radiation.

a phase-slip flux qubit.
The phase slip qubit consists of a superconducting loop with an embedded QPS wire, see Fig. 7, left. In the superconducting state the flux in the loop is fixed and can only change by a phase slip event. The qubit is very similar to the well known Josephson junction based flux qubit. In case of a vanishing E_s, the energy spectrum of the loop is given by $E = (\Phi_{ext} - N\Phi_0)^2/2L$, where L is the inductance and N the number of flux quanta in the loop, depicted as dashed parabolas in the energy spectrum Fig. 7.
If an external flux $\Phi/\Phi_0 = 0.5$ is applied to the qubit with a non-vanishing phase slip energy E_s, a flux vortex is allowed to periodically enter (or leave) the superconducting loop. At $0.5\Phi_0$ the neighboring flux state degeneracy is lifted and a gap for the two relevant qubit states separated by E_s opens in the spectrum.
Astafiev *et al.* showed exactly this behavior by strongly coupling a QPS-qubit to a superconducting resonator (Fig. 7, left sketch) and measuring the resonator transmission spectrum depending on applied magnetic flux. They demonstrated that quantum phase slips can be induced by flux bias driving, thus non-stochastical *coherent quantum phase slips* are possible. For the first time it was shown experimentally, that there can be a coherent coupling of flux states across a QPS junction in exact duality to the coherent coupling of charge states across a Josephson junction. Furthermore, E_s was for the first time directly measured, confirming theoretical models for QPS in the weak phase slip regime. Astafiev *et al.* used a QPS qubit where loop and wire were made from a highly resistive, amorphous In$\emptyset$ film with a superconducting transition temperature of 2.7 K. The wire had a length of 400 nm and width of 40 nm, defined by e-beam lithography. E_s was measured to about 5 GHz with an ξ estimate in the range of 10-30 nm. All these parameters are accessible by conventional fabrication techniques, encouraging for more QPS related experiments.

4.3 Constant current steps

Assuming the duality between the Josephson junction and the phase slip junction outlined above is correct, there must be an equivalent to the constant voltage steps found in the $I-V$ characteristics of the Josephson junction under microwave radiation (Shapiro steps). If found, they might be of scientific and technological interest, due to their potential for being used as a current standard.

The QPS junction in the strong phase slip regime embedded in a dissipative environment, see Fig. 8, left, can be described by a semiclassical RCSJ type circuit model with I and ϕ replaced by their canonical conjugated variables V and q. The voltage drop over a QPS junction is then given by

$$V(t) = V_c \sin(2\pi q) + 2e\left(L\frac{\mathrm{d}^2 q}{\mathrm{d}t^2} + R\frac{\mathrm{d}q}{\mathrm{d}t}\right)$$

The model is of the well known tilted washboard potential type, with the tilt V and the position of the virtual particle q [58]. If an oscillating voltage with a frequency ν, phase locked on the QPS rate, is applied to a QPS junction, plateaus of constant current develop in the $I-V$ characteristic at a current $I = n\,2e\,\nu$, where $n = 1, 2, 3, ...$ is the step, see Fig. 8, right plot.
First experiments looking for current steps in QPS junctions under microwave radiation have been carried out, but were not successfully observing the steps, see e.g. Refs. [64, 65]. In the ultra-low temperature experiments (T¡100 mK), the heat produced by the high ohmic NiCr on-chip bias resisters was found to be significant. This prevents the QPS wire to be intrinsically cold enough and the conductance not being dominated by parasitic quasiparticle channels.

The existence of a fundamental and direct current-frequency relation utilizing QPS wires remains therefore an open experimental question.

References

[1] DiVincenzo, D.P. (2000) The Physical Implementation of Quantum Computation. *Fortschr. Phys.–Progress of Physics*, **48**, 771, doi:10.1002/1521-3978(200009)48:9/11⟨771::AID-PROP771⟩3.0.CO;2-E. URL `http://dx.doi.org/10.1002/1521-3978(200009)48:9/11<771::AID-PROP771>3.0.CO;2-E`

[2] Clark, T.D., Prance, R.J., and Grassie, A.D.C. (1980) Feasibility of hybrid Josephson field effect transistors. *J. Appl. Phys.*, **51** (5), 2736–2743, doi:10.1063/1.327935. URL `http://dx.doi.org/10.1063/1.327935`.

[3] Kleinsasser, A.W. (1991) Critical currents of semiconductor-coupled Josephson weak links. *IEEE Trans. Mag.*, **27** (2), 2589–2593, doi:10.1109/20.133745. URL `http://dx.doi.org/10.1109/20.133745`.

[4] Becker, T., Mück, M., and Heiden, C. (1995) Transport properties of niobium-silicon superconductor-semiconductor junctions. *Physica B*, **204** (1-4), 183–189, doi:10.1016/0921-4526(94)00261-s. URL `http://dx.doi.org/10.1016/0921-4526(94)00261-s`.

[5] Doh, Y.J., van Dam, J.A., Roest, A.L., Bakkers, E.P.A.M., Kouwenhoven, L.P., and De Franceschi, S. (2005) Tunable Supercurrent Through Semiconductor Nanowires. *Science*, **309** (5732), 272–275, doi:10.1126/science.1113523. URL `http://dx.doi.org/10.1126/science.1113523`.

[6] van Dam, J.A., Nazarov, Y.V., Bakkers, E.P.A.M., De Franceschi, S., and Kouwenhoven, L.P. (2006) Supercurrent reversal in quantum dots. *Nature (London)*, **442** (7103), 667–670, doi:10.1038/nature05018. URL `http://dx.doi.org/10.1038/nature05018`.

[7] Xiang, J., Vidan, A., Tinkham, M., Westervelt, R.M., and Lieber, C.M. (2006) Ge/Si nanowire mesoscopic Josephson junctions. *Nat Nano*, **1** (3), 208–213, doi:10.1038/nnano.2006.140. URL `http://dx.doi.org/10.1038/nnano.2006.140`.

[8] Frielinghaus, R., Batov, I.E., Weides, M., Kohlstedt, H., Calarco, R., and Schäpers, T. (2010) Josephson supercurrent in Nb/InN-nanowire/Nb junctions. *Appl. Phys. Lett.*, **96** (13), 132 504, doi:10.1063/1.3377897\%2522. URL `http://dx.doi.org/10.1063/1.3377897%2522`.

[9] Jarillo-Herrero, P., van Dam, J.A., and Kouwenhoven, L.P. (2006) Quantum supercurrent transistors in carbon nanotubes. *Nature (London)*, **439** (7079), 953–956, doi:10.1038/nature04550. URL `http://dx.doi.org/10.1038/nature04550`.

[10] Voss, R.F., Laibowitz, R.B., and Broers, A.N. (1980) Niobium nanobridge dc SQUID. *Appl. Phys. Lett.*, **37** (7), 656–658, doi:10.1063/1.92026. URL http://dx.doi.org/10.1063/1.92026.

[11] Ketchen, M.B., Kopley, T., and Ling, H. (1984) Miniature SQUID susceptometer. *Appl. Phys. Lett.*, **44** (10), 1008–1010, doi:10.1063/1.94601. URL http://dx.doi.org/10.1063/1.94601.

[12] Foley, C.P. and Hilgenkamp, H. (2009) Why NanoSQUIDs are important: an introduction to the focus issue. *Supercond. Sci. Technol.*, **22** (6), 064 001, doi:10.1088/0953-2048/22/6/064001. URL http://dx.doi.org/10.1088/0953-2048/22/6/064001.

[13] Cleuziou, J.P., Wernsdorfer, W., Bouchiat, V., Ondarcuhu, T., and Monthioux, M. (2006) Carbon nanotube superconducting quantum interference device. *Nature Nanotechnology*, **1** (1), 53–59, doi:10.1038/nnano.2006.54. URL http://dx.doi.org/10.1038/nnano.2006.54.

[14] Leijnse, M. and Flensberg, K. (2012) Introduction to topological superconductivity and Majorana fermions. *Semiconductor Science and Technology*, **27** (12), 124 003, doi:10.1088/0268-1242/27/12/124003. URL http://dx.doi.org/10.1088/0268-1242/27/12/124003.

[15] Alicea, J. (2010) Majorana fermions in a tunable semiconductor device. *Phys. Rev. B*, **81** (12), 125 318, doi:10.1103/physrevb.81.125318. URL http://dx.doi.org/10.1103/physrevb.81.125318.

[16] Sau, J.D., Lutchyn, R.M., Tewari, S., and Sarma, S.D. (2010) Generic New Platform for Topological Quantum Computation Using Semiconductor Heterostructures. *Phys. Rev. Lett.*, **104**, 040 502, doi:10.1103/physrevlett.104.040502. URL http://dx.doi.org/10.1103/physrevlett.104.040502.

[17] Potter, A.C. and Lee, P.A. (2012) Topological superconductivity and Majorana fermions in metallic surface states. *Phys. Rev. B*, **85**, 094 516, doi:10.1103/physrevb.85.094516. URL http://dx.doi.org/10.1103/physrevb.85.094516.

[18] Mourik, V., Zuo, K., Frolov, S.M., Plissard, S.R., Bakkers, E.P.A.M., and Kouwenhoven, L.P. (2012) Signatures of Majorana Fermions in Hybrid Superconductor-Semiconductor Nanowire Devices. *Science*, **336** (6084), 1003, doi:10.1126/science.1222360. URL http://dx.doi.org/10.1126/science.1222360.

[19] Read, N. (2012) Topological phases and quasiparticle braiding. *Physics Today*, **65** (7), 38, doi:10.1063/PT.3.1641. URL http://link.aip.org/link/?PTO/65/38/1.

[20] Nakamura, Y., Pashkin, Y., and Tsai, J.S. (1999) Coherent control of macroscopic quantum states in a single-Cooper-pair box. *Nature*, **398** (6730), 786, doi:10.1038/19718. URL http://dx.doi.org/10.1038/19718.

[21] Mooij, J.E., Orlando, T.P., Levitov, L., Tian, L., van der Wal, C.H., and Lloyd, S. (1999) Josephson persistent-current qubit. *Science*, **285**, 1036, doi:10.1126/science.285.5430.1036. URL http://dx.doi.org/10.1126/science.285.5430.1036.

[22] Martinis, J.M., Nam, S., Aumentado, J., and Urbina, C. (2002) Rabi oscillations in a large Josephson-junction qubit. *Phys. Rev. Lett.*, **89** (11), 117901, doi:10.\%25201103/PhysRevLett.\%252089.\%2520117901. URL http://dx.doi.org/10.%25201103/PhysRevLett.%252089.%2520117901.

[23] Vion, D., Aassime, A., Cottet, A., Joyez, P., Pothier, H., Urbina, C., Esteve, D., and Devoret, M.H. (2002) Manipulating the quantum state of an electrical circuit. *Science*, **269**, 886, doi:10.1126/science.1069372. URL http://dx.doi.org/10.1126/science.1069372.

[24] Steffen, M., Kumar, S., DiVincenzo, D.P., Rozen, J.R., Keefe, G.A., Rothwell, M.B., and Ketchen, M.B. (2010) High-Coherence Hybrid Superconducting Qubit. *Phys. Rev. Lett.*, **105**, 100 502, doi:10.1103/physrevlett.105.100502. URL http://dx.doi.org/10.1103/physrevlett.105.100502.

[25] Zorin, A.B. and Chiarello, F. (2009) Superconducting phase qubit based on the Josephson oscillator with strong anharmonicity. *Phys. Rev. B*, **80** (21), 214 535, doi:10.1103/physrevb.80.214535. URL http://dx.doi.org/10.1103/physrevb.80.214535.

[26] Koch, J., Yu, T.M., Gambetta, J., Houck, A.A., Schuster, D.I., Majer, J., Blais, A., Devoret, M.H., Girvin, S.M., and Schoelkopf, R.J. (2007) Charge-insensitive qubit design derived from the Cooper pair box. *Phys. Rev. A*, **76** (4), 042 319, doi:10.1103/PhysRevA.76.042319. URL http://link.aps.org/doi/10.1103/PhysRevA.76.042319.

[27] Day, P.K., LeDuc, H.G., Mazin, B.A., Vayonakis, A., and Zmuidzinas, J. (2003) A broadband superconducting detector suitable for use in large arrays. *Nature (London)*, **425** (6960), 817–821, doi:10.1038/nature02037. URL http://dx.doi.org/10.1038/nature02037.

[28] Megrant, A., Neill, C., Barends, R., Chiaro, B., Chen, Y., Feigl, L., Kelly, J., Lucero, E., Mariantoni, M., O'Malley, P.J.J., Sank, D., Vainsencher, A., Wenner, J., White, T.C., Yin, Y., Zhao, J., Palmstrom, C.J., Martinis, J.M., and Cleland, A.N. (2012) Planar superconducting resonators with internal quality factors above one million. *Appl. Phys. Lett.*, **100** (11), 113 510, doi:10.1063/1.3693409. URL http://dx.doi.org/10.1063/1.3693409.

[29] Barends, R., Vercruyssen, N., Endo, A., de Visser, P.J., Zijlstra, T., Klapwijk, T.M., Diener, P., Yates, S.J.C., and Baselmans, J.J.A. (2010) Minimal resonator loss for circuit quantum electrodynamics. *Appl. Phys. Lett.*, **97** (2), 023 508, doi:10.1063/1.3458705. URL http://dx.doi.org/10.1063/1.3458705.

[30] Vissers, M.R., Gao, J., Wisbey, D.S., Hite, D.A., Tsuei, C.C., Corcoles, A.D., Steffen, M., and Pappas, D.P. (2010) Low loss superconducting titanium nitride coplanar waveguide resonators. *Appl. Phys. Lett.*, **97** (23), 232 509, doi:10.1063/1.3517252. URL http://dx.doi.org/10.1063/1.3517252.

[31] Sandberg, M., Vissers, M.R., Kline, J.S., Weides, M., Gao, J., Wisbey, D.S., and Pappas, D.P. (2012) Etch induced microwave losses in titanium nitride superconducting resonators. *Appl. Phys. Lett.*, **100** (26), 262 605, doi:10.1063/1.4729623. URL http://dx.doi.org/10.1063/1.4729623.

[32] Paik, H., Schuster, D.I., Bishop, L.S., Kirchmair, G., Catelani, G., Sears, A.P., Johnson, B.R., Reagor, M.J., Frunzio, L., Glazman, L.I., Girvin, S.M., Devoret, M.H., and Schoelkopf, R.J. (2011) Observation of High Coherence in Josephson Junction Qubits Measured in a Three-Dimensional Circuit QED Architecture. *Phys. Rev. Lett.*, **107**, 240 501, doi:10.1103/physrevlett.107.240501. URL http://dx.doi.org/10.1103/physrevlett.107.240501.

[33] Veselago, V.G. (1968) The Electrodynamics Of Substances With Simultaneously Negative Values Of ϵ And μ. *Soviet Physics Uspekhi*, **10** (4), 509–514, doi:10.1070/pu1968v010n04abeh003699. URL http://dx.doi.org/10.1070/pu1968v010n04abeh003699.

[34] Pendry, J.B., Holden, A.J., Robbins, D.J., and Stewart, W.J. (1999) Magnetism from conductors and enhanced nonlinear phenomena. *IEEE Transactions on Microwave Theory and Techniques*, **47** (11), 2075–2084, doi:10.1109/22.798002. URL http://dx.doi.org/10.1109/22.798002.

[35] Shelby, R.A., Smith, D.R., and Schultz, S. (2001) Experimental Verification of a Negative Index of Refraction. *Science*, **292** (5514), 77–79, doi:10.1126/science.1058847. URL http://dx.doi.org/10.1126/science.1058847.

[36] Ricci, M., Orloff, N., and Anlage, S.M. (2005) Superconducting metamaterials. *Appl. Phys. Lett.*, **87** (3), 034 102, doi:10.1063/1.1996844. URL http://dx.doi.org/10.1063/1.1996844.

[37] Castellanos-Beltran, M.A., Irwin, K.D., Hilton, G.C., Vale, L.R., and Lehnert, K.W. (2008) Amplification and squeezing of quantum noise with a tunable Josephson metamaterial. *Nat Phys*, **4** (12), 929–931, doi:10.1038/nphys1090. URL http://dx.doi.org/10.1038/nphys1090.

[38] Astafiev, O., Inomata, K., Niskanen, A.O., Yamamoto, T., Pashkin, Y., Nakamura, Y., and Tsai, J.S. (2007) Single artificial-atom lasing. *Nature (London)*, **449** (7162), 588–590, doi:10.1038/nature06141. URL http://dx.doi.org/10.1038/nature06141.

[39] Du, C., Chen, H., and Li, S. (2006) Quantum left-handed metamaterial from superconducting quantum-interference devices. *Phys. Rev. B*, **74**, 113 105, doi:10.1103/physrevb.74.113105. URL http://dx.doi.org/10.1103/physrevb.74.113105.

[40] Rakhmanov, A.L., Zagoskin, A.M., Savel'ev, S., and Nori, F. (2008) Quantum metamaterials: Electromagnetic waves in a Josephson qubit line. *Phys. Rev. B*, **77** (14), 144 507, doi:10.1103/physrevb.77.144507. URL http://dx.doi.org/10.1103/physrevb.77.144507.

[41] Zhou, L., Gao, Y.B., Song, Z., and Sun, C.P. (2008) Coherent output of photons from coupled superconducting transmission line resonators controlled by charge qubits. *Phys. Rev. A*, **77**, 013 831, doi:10.1103/physreva.77.013831. URL http://dx.doi.org/10.1103/physreva.77.013831.

[42] Jaynes, E.T. and Cummings, F.W. (1963) Comparison of quantum and semiclassical radiation theories with application to the beam maser. *Proceedings of the IEEE*, **51** (1), 89, doi:10.1109/proc.1963.1664. URL http://dx.doi.org/10.1109/proc.1963.1664.

[43] Blais, A., Huang, R.S., Wallraff, A., Girvin, S.M., and Schoelkopf, R.J. (2004) Cavity quantum electrodynamics for superconducting electrical circuits: An architecture for quantum computation. *Phys. Rev. A*, **69** (6), 062 320, doi:10.1103/physreva.69.062320. URL http://dx.doi.org/10.1103/physreva.69.062320.

[44] Tavis, M. and Cummings, F.W. (1968) Exact Solution for an N-Molecule Radiation-Field Hamiltonian. *Physical Review Online Archive (Prola)*, **170** (2), 379, doi:10.1103/physrev.170.379. URL http://dx.doi.org/10.1103/physrev.170.379.

[45] Dicke, R.H. (1954) Coherence in Spontaneous Radiation Processes. *Physical Review Online Archive (Prola)*, **93** (1), 99, doi:10.1103/physrev.93.99. URL http://dx.doi.org/10.1103/physrev.93.99.

[46] Bonifacio, R. and Lugiato, L.A. (1975) Cooperative radiation processes in two-level systems: Superfluorescence. *Physical Review A*, **11** (5), 1507, doi:10.1103/physreva.11.1507. URL http://dx.doi.org/10.1103/physreva.11.1507.

[47] Tsomokos, D.I., Hartmann, M.J., Huelga, S.F., and Plenio, M.B. (2007) Entanglement dynamics in chains of qubits with noise and disorder. *New Journal of Physics*, **9** (3), 79, doi:10.1088/1367-2630/9/3/079. URL http://dx.doi.org/10.1088/1367-2630/9/3/079.

[48] Delanty, M., Rebić, S., and Twamley, J. (2011) Superradiance and phase multistability in circuit quantum electrodynamics. *New Journal of Physics*, **13** (5), 053 032, doi:10.1088/1367-2630/13/5/053032. URL http://dx.doi.org/10.1088/1367-2630/13/5/053032.

[49] Ian, H., Liu, Y.X., and Nori, F. (2012) Excitation spectrum for an inhomogeneously dipole-field-coupled superconducting qubit chain. *Physical Review A*, **85**, 053 833, doi:10.1103/physreva.85.053833. URL http://dx.doi.org/10.1103/physreva.85.053833.

[50] Astafiev, O., Zagoskin, A.M., Abdumalikov, A.A., Pashkin, Y.A., Yamamoto, T., Inomata, K., Nakamura, Y., and Tsai, J.S. (2010) Resonance fluorescence of a single artificial atom. *Science (New York, N.Y.)*, **327** (5967), 840–843, doi:10.1126/science.1181918. URL http://dx.doi.org/10.1126/science.1181918.

[51] Abdumalikov, A.A., Astafiev, O., Zagoskin, A.M., Yu, Nakamura, Y., and Tsai, J.S. (2010) Electromagnetically Induced Transparency on a Single Artificial Atom. *Phys. Rev. Lett.*, **104** (19), 193 601, doi:10.1103/physrevlett.104.193601. URL http://dx.doi.org/10.1103/physrevlett.104.193601.

[52] Kelly, W.R., Dutton, Z., Schlafer, J., Mookerji, B., Ohki, T.A., Kline, J.S., and Pappas, D.P. (2010) Direct Observation of Coherent Population Trapping in a Superconducting Artificial Atom. *Phys. Rev. Lett.*, **104**, 163 601, doi:10.1103/physrevlett.104.163601. URL http://dx.doi.org/10.1103/physrevlett.104.163601.

[53] Hoi, I.C., Wilson, C.M., Johansson, G., Palomaki, T., Peropadre, B., and Delsing, P. (2011) Demonstration of a Single-Photon Router in the Microwave Regime. *Phys. Rev. Lett.*, **107**, 073 601, doi:10.1103/physrevlett.107.073601. URL http://dx.doi.org/10.1103/physrevlett.107.073601.

[54] Giordano, N. (1988) Evidence for macroscopic quantum tunneling in one-dimensional superconductors. *Phys. Rev. Lett.*, **61**, 2137–2140, doi:10.1103/PhysRevLett.61.2137. URL http://link.aps.org/doi/10.1103/PhysRevLett.61.2137.

[55] Bezryadin, A., Lau, C.N., and Tinkham, M. (2000) Quantum suppression of superconductivity in ultrathin nanowires. *Nature*, **404** (6781), 971–974, doi:10.1038/35010060. URL http://dx.doi.org/10.1038/35010060.

[56] Lau, C.N., Markovic, N., Bockrath, M., Bezryadin, A., and Tinkham, M. (2001) Quantum phase slips in superconducting nanowires. *Phys. Rev. Lett.*, **87**, 217 003, doi:10.1103/PhysRevLett.87.217003. URL http://link.aps.org/doi/10.1103/PhysRevLett.87.217003.

[57] Arutyunov, K., Golubev, D., and Zaikin, A. (2008) Superconductivity in one dimension. *Physics Reports*, **464**, 1 – 70, doi:10.1016/j.physrep.2008.04.009. URL http://www.sciencedirect.com/science/article/pii/S0370157308001609.

[58] Mooij, J.E. and Nazarov, Y.V. (2006) Superconducting nanowires as quantum phase-slip junctions. *Nat Phys*, **2** (3), 169–172, doi:10.1038/nphys234. URL http://dx.doi.org/10.1038/nphys234.

[59] Zaikin, A.D., Golubev, D.S., van Otterlo, A., and Zimányi, G.T. (1997) Quantum phase slips and transport in ultrathin superconducting wires. *Phys. Rev. Lett.*, **78**, 1552–1555, doi:10.1103/PhysRevLett.78.1552. URL http://link.aps.org/doi/10.1103/PhysRevLett.78.1552.

[60] Golubev, D.S. and Zaikin, A.D. (2001) Quantum tunneling of the order parameter in superconducting nanowires. *Phys. Rev. B*, **64**, 014 504, doi:10.1103/PhysRevB.64.014504. URL http://link.aps.org/doi/10.1103/PhysRevB.64.014504.

[61] Büchler, H.P., Geshkenbein, V.B., and Blatter, G. (2004) Quantum fluctuations in thin superconducting wires of finite length. *Phys. Rev. Lett.*, **92**, 067 007, doi:10.1103/PhysRevLett.92.067007. URL http://link.aps.org/doi/10.1103/PhysRevLett.92.067007.

[62] Mooij, J.E. and Harmans, C.J.P.M. (2005) Phase-slip flux qubits. *New Journal of Physics*, **7** (1), 219. URL http://stacks.iop.org/1367-2630/7/i=1/a=219.

[63] Astafiev, O.V., Ioffe, L.B., Kafanov, S., Pashkin, Y.A., Arutyunov, K.Y., Shahar, D., Cohen, O., and Tsai, J.S. (2012) Coherent quantum phase slip. *Nature*, **484** (7394), 355–358, doi:10.1038/nature10930. URL http://dx.doi.org/10.1038/nature10930.

[64] Hongisto, T.T. and Zorin, A.B. (2012) Single-charge transistor based on the charge-phase duality of a superconducting nanowire circuit. *Phys. Rev. Lett.*, **108**, 097 001, doi:10.1103/PhysRevLett.108.097001. URL http://link.aps.org/doi/10.1103/PhysRevLett.108.097001.

[65] Webster, C.H., Fenton, J.C., Hongisto, T.T., Giblin, S.P., Zorin, A.B., and Warburton, P.A. (2013) Nbsi nanowire quantum phase-slip circuits: dc supercurrent blockade, microwave measurements, and thermal analysis. *Phys. Rev. B*, **87**, 144 510, doi:10.1103/PhysRevB.87.144510. URL http://link.aps.org/doi/10.1103/PhysRevB.87.144510.